Monthly Notices
of the
ROYAL ASTRONOMICAL SOCIETY

MNRAS **463,** 4469–4480 (2016)
Advance Access publication 2016 September 14

doi:10.1093/mnras/stw2325

The awakening of the γ-ray narrow-line Seyfert 1 galaxy PKS 1502+036

F. D'Ammando,[1,2]★ M. Orienti,[2] J. Finke,[3] T. Hovatta,[4] M. Giroletti,[2] W. Max-Moerbeck,[5] T. J. Pearson,[6] A. C. S. Readhead,[6] R. A. Reeves[7] and J. L. Richards[8]

[1]*Dip. di Fisica e Astronomia, Università di Bologna, Via Ranzani 1, I-40127 Bologna, Italy*
[2]*INAF – Istituto di Radioastronomia, Via Gobetti 101, I-40129 Bologna, Italy*
[3]*US Naval Research Laboratory, Code 7653, 4555 Overlook Ave. SW, Washington, DC 20375-5352, USA*
[4]*Aalto University Metsähovi Radio Observatory, Metsähovintie 114, FI-02540 Kylmälä, Finland*
[5]*Max-Planck-Institut für Radioastronomie, Auf dem Hügel 69, D-53121 Bonn, Germany*
[6]*Cahill Center for Astronomy and Astrophysics, California Institute of Technology 1200 E. California Blvd., Pasadena, CA 91125, USA*
[7]*Departamento de Astronomía, CePIA, Universidad de Concepcion, Casilla 160-C Concepcion, Chile*
[8]*Department of Physics, Purdue University, 525 Northwestern Avenue, West Lafayette, IN 47907, USA*

Accepted 2016 September 13. Received 2016 September 12; in original form 2016 June 22

ABSTRACT

After a long low-activity period, a γ-ray flare from the narrow-line Seyfert 1 PKS 1502+036 ($z = 0.4089$) was detected by the Large Area Telescope (LAT) on board *Fermi* in 2015. On 2015 December 20, the source reached a daily peak flux, in the 0.1–300 GeV band, of $(93 \pm 19) \times 10^{-8}$ ph cm^{-2} s^{-1}, attaining a flux of $(237 \pm 71) \times 10^{-8}$ ph cm^{-2} s^{-1} on 3-h time-scales, which corresponds to an isotropic luminosity of $(7.3 \pm 2.1) \times 10^{47}$ erg s^{-1}. The γ-ray flare was not accompanied by significant spectral changes. We report on multiwavelength radio-to-γ-ray observations of PKS 1502+036 during 2008 August–2016 March by *Fermi*-LAT, *Swift*, *XMM–Newton*, Catalina Real-Time Transient Survey and the Owens Valley Radio Observatory (OVRO). An increase in activity was observed on 2015 December 22 by *Swift* in optical, UV and X-rays. The OVRO 15 GHz light curve reached the highest flux density observed from this source on 2016 January 12, indicating a delay of about three weeks between the γ-ray and 15 GHz emission peaks. This suggests that the γ-ray-emitting region is located beyond the broad-line region. We compared the spectral energy distribution (SED) of an average activity state with that of the flaring state. The two SED, with the high-energy bump modelled as an external Compton component with seed photons from a dust torus, could be fitted by changing the electron distribution parameters as well as the magnetic field. The fit of the disc emission during the average state constrains the black hole mass to values lower than 10^8 M$_\odot$. The SED, high-energy emission mechanisms and γ-ray properties of the source resemble those of a flat spectrum radio quasar.

Key words: galaxies: individual: PKS 1502+036 – galaxies: jets – galaxies: nuclei – galaxies: Seyfert – gamma-rays: general.

1 INTRODUCTION

Relativistic jets are mainly produced by radio-loud active galactic nuclei (AGN) such as blazars and radio galaxies hosted in giant elliptical galaxies (Blandford & Rees 1978). The discovery by the Large Area Telescope (LAT) on-board the *Fermi Gamma-ray Space Telescope* of variable γ-ray emission from narrow-line Seyfert 1 (NLSy1) galaxies revealed the presence of a new class of AGN with relativistic jets (e.g. Abdo et al. 2009b,a; D'Ammando et al. 2012, 2015b). Considering that NLSy1 are usually hosted in spiral galaxies (e.g. Deo, Crenshow & Kraemer 2006), the presence of a relativistic jet in these sources seems to be in contrast to the paradigm that the formation of relativistic jets could happen in elliptical galaxies only (Böttcher & Dermer 2002; Marscher 2010). This finding poses intriguing questions about the nature of these objects and the formation of relativistic jets. In particular, one of the debated properties of NLSy1 is their relatively small black hole (BH) mass ($M_{\rm BH} = 10^{6-8}$ M$_\odot$) in comparison to blazars and radio galaxies. It was suggested that the BH masses of NLSy1 are underestimated due to either the effect of radiation pressure (Marconi et al. 2008) or the projection effects (Baldi et al. 2016). Higher BH masses than those derived by the virial method (e.g. Yuan et al. 2008) are in agreement with the values estimated by

★ E-mail: dammando@ira.inaf.it

modelling the optical/UV data with a Shakura and Sunyaev disc spectrum (Calderone et al. 2013).

PKS 1502+036 has been classified as an NLSy1 on the basis of its optical spectrum: full width at half-maximum, FWHM (H β) = (1082 ± 113) km s^{-1}, [O III]/H $\beta \sim 1.1$, and a strong Fe II bump (Yuan et al. 2008). Among the radio-loud NLSy1, PKS 1502+036 has one of the highest radio-loudness values (RL = 1549).[1] The source exhibits a compact core-jet structure on pc-scales, with the radio emission dominated by the core component, while the jet-like feature accounts for only 4 per cent of the total flux density (Orienti, D'Ammando & Giroletti 2012; D'Ammando et al. 2013b). Simultaneous multifrequency Very Large Array observations carried out at various epochs showed substantial spectral and flux density variability. Lister et al. (2016) analysing the Monitoring Of Jets in Active galactic nuclei with VLBA Experiments (MOJAVE) images of PKS 1502+036 collected during 2010–2013 found a jet component moving at sub-luminal speed (i.e. 1.1 ± 0.4 c). Optical intra-day variability with a flux amplitude of about 10 per cent was reported for PKS 1502+036 by Paliya et al. (2013). In infrared bands, a variation of 0.1–0.2 mag in 180 d was observed by the *Wide-field Infrared Survey Explorer* (Jiang et al. 2012).

In the γ-ray energy band, PKS 1502+036 was not detected in the 1990s by the Energetic Gamma-Ray Experiment Telescope on board the *Compton Gamma Ray Observatory* at E > 100 MeV (Hartman et al. 1999). On the other hand, the source has been included in the first, second, and third *Fermi*-LAT source catalogues (1FGL, 2FGL, 3FGL; Abdo et al. 2010; Nolan et al. 2012; Acero et al. 2015). No significant increase of γ-ray flux was observed between 2008 August and 2012 November (D'Ammando et al. 2013b). In 2015 December, γ-ray flaring activity from PKS 1502+036 was detected on a daily time-scale by *Fermi*-LAT (D'Ammando & Ciprini 2015), confirmed at lower energies by *Swift* observations (D'Ammando 2015).

In this paper, we discuss the flaring activity of PKS 1502+036 observed in 2015 December–2016 January in comparison to the 2008–2015 data collected from radio to γ-rays. The paper is organized as follows. In Section 2, we report the LAT data analysis and results. In Section 3, we present the results of the *Swift* and *XMM–Newton* observations. Optical data collected by the Catalina Real-Time Transient Survey (CRTS) and radio data collected by the 40 m Owens Valley Radio Observatory (OVRO) single-dish telescope are reported in Section 4. In Section 5, we discuss the properties and the modelling of the spectral energy distribution (SED) of the source during an average activity state and the high-activity state. Finally, we draw our conclusions in Section 6. Throughout the paper, a Λ cold dark matter cosmology with $H_0 = 71$ km s^{-1} Mpc^{-1}, $\Omega_\Lambda = 0.73$ and $\Omega_m = 0.27$ (Komatsu et al. 2011) is adopted. The corresponding luminosity distance at $z = 0.4089$ (i.e. the source redshift; Schneider et al. 2010) is $d_L = 2220$ Mpc. In this paper, the quoted uncertainties are given at the 1σ level, unless otherwise stated, and the photon indices are parametrized as $dN/dE \propto E^{-\Gamma}$ with $\Gamma = s+1$ (s is the spectral index).

2 *Fermi*-LAT DATA: ANALYSIS AND RESULTS

The *Fermi*-LAT is a pair-conversion telescope operating from 20 MeV to > 300 GeV. Further details about the *Fermi*-LAT are given in Atwood et al. (2009).

The LAT data used in this paper were collected from 2008 August 5 (MJD 54683) to 2016 March 24 (MJD 57471). During this time, the LAT instrument operated almost entirely in survey mode. The Pass 8 data (Atwood et al. 2013), based on a complete and improved revision of the entire LAT event-level analysis, were used. The analysis was performed with the SCIENCETOOLS software package version v10r0p5. Only events belonging to the 'Source' class (`evclass=128, evtype=3`) were used. We selected only events within a maximum zenith angle of 90° to reduce contamination from the Earth limb γ-rays, which are produced by cosmic rays interacting with the upper atmosphere. The spectral analysis was performed with the instrument response functions `P8R2_SOURCE_V6` using a binned maximum-likelihood method implemented in the Science tool `gtlike`. Isotropic ('iso_source_v06.txt') and Galactic diffuse emission ('gll_iem_v06.fit') components were used to model the background (Acero et al. 2016).[2] The normalization of both components was allowed to vary freely during the spectral fitting.

We analysed a region of interest of 30° radius centred at the location of PKS 1502+036. We evaluated the significance of the γ-ray signal from the source by means of a maximum-likelihood test statistic (TS) defined as TS = 2 × (logL_1 − logL_0), where L is the likelihood of the data given the model with (L_1) or without (L_0) a point source at the position of PKS 1502+036 (e.g. Mattox et al. 1996). The source model used in `gtlike` includes all the point sources from the 3FGL catalogue that fall within 40° of PKS 1502+036. The spectra of these sources were parametrized by a power law (PL), a log-parabola (LP), or a super exponential cut-off, as in the 3FGL catalogue. We also included new candidates within 10° of PKS 1502+036 from a preliminary source list using 7 yr of Pass 8 data.

A first maximum-likelihood analysis was performed over the whole period to remove from the model the sources having TS < 25. A second maximum-likelihood analysis was performed on the updated source model. In the fitting procedure, the normalization factors and the spectral parameters of the sources lying within 10° of PKS 1502+036 were left as free parameters. For the sources located between 10° and 40° from our target, we kept the normalization and the spectral shape parameters fixed to the values from the 3FGL catalogue.

Integrating over 2008 August 5–2016 March 24, the fit with a PL model, $dN/dE \propto (E/E_0)^{-\Gamma_\gamma}$, as in the 3FGL catalogue, results in TS = 1067 in the 0.1–300 GeV energy range, with an integrated average flux of (4.40 ± 0.21) × 10^{-8} ph cm^{-2} s^{-1} and a photon index of $\Gamma_\gamma = 2.62 \pm 0.04$. The corresponding apparent isotropic γ-ray luminosity is (1.3 ± 0.1) × 10^{46} erg s^{-1}.

Fig. 1 shows the γ-ray light curve of PKS 1502+036 for 2008 August–2016 March using a PL model and 90-d time bins. For each time bin, the spectral parameters of PKS 1502+036 and all sources within 10° of it were frozen to the values resulting from the likelihood analysis over the entire period. When TS < 10, 2σ upper limits were calculated. The statistical uncertainty in the fluxes is larger than the systematic uncertainty (Ackermann et al. 2012) and only the former is considered in this paper.

Until September 2015, no significant variability was observed from PKS 1502+036 on a 90-d time-scale. The 0.1–300 GeV flux ranged within the range (2–7) × 10^{-8} ph cm^{-2} s^{-1}. An increase of activity was observed during 2015 September 29–December 25, when the source reached a 90-d averaged flux (0.1–300 GeV) of (11.5 ± 1.2) × 10^{-8} ph cm^{-2} s^{-1}, a factor of 2.5 higher than the

[1] RL being defined as the ratio between the 1.4 GHz and 4400 Å rest-frame flux densities.

[2] http://fermi.gsfc.nasa.gov/ssc/data/access/lat/BackgroundModels.html

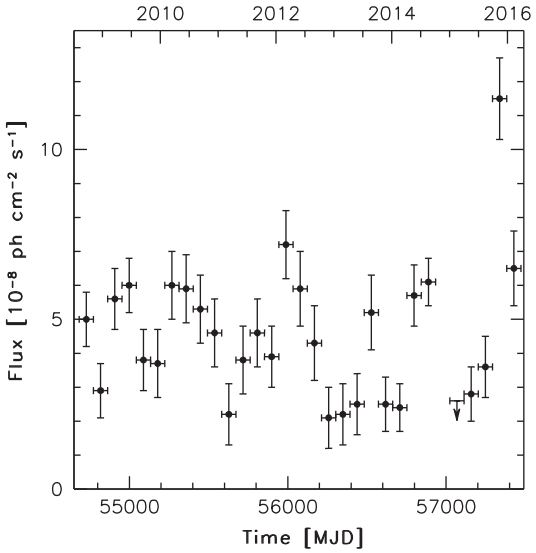

Figure 1. Integrated flux light curve of PKS 1502+036 obtained in the 0.1–300 GeV energy range during 2008 August 5–2016 March 24 (MJD 54683–57471) with 90-d time bins. Arrow refers to 2σ upper limit on the source flux. Upper limits are computed when TS < 10.

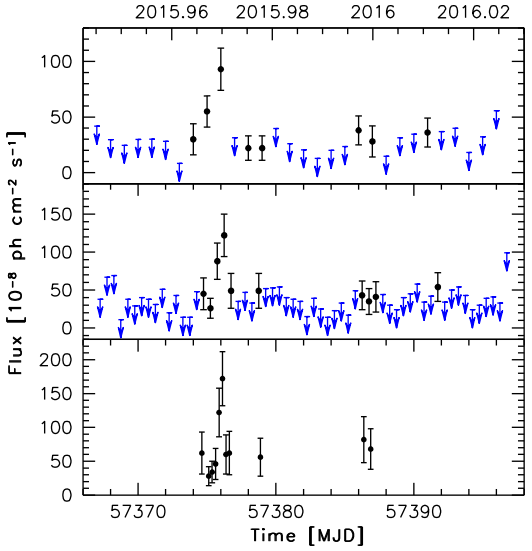

Figure 2. Integrated flux light curve of PKS 1502+036 obtained by *Fermi*-LAT in the 0.1–300 GeV energy range during 2015 December 11–2016 January 9 (MJD 57367–57396), with 1-d time bins (top panel), 12-h time bins (middle panel), and 6-h time bins (bottom panel). Arrows refer to 2σ upper limits on the source flux. Upper limits are computed when TS < 10. In the bottom panel, upper limits are not shown.

average γ-ray flux. Leaving the photon index of our target (and of all sources within 10° of our target) free to vary, the fit for PKS 1502+036 results in TS = 155 and a photon index $\Gamma_\gamma = 2.57 \pm 0.11$, suggesting no spectral variations during the high-activity state. In order to test for curvature in the γ-ray spectrum of PKS 1502+036, an alternative spectral model to the PL, an LP, $dN/dE \propto E/E_0^{-\alpha-\beta\ \log(E/E_0)}$, was used for the fit. We obtain a spectral slope $\alpha = 2.50 \pm 0.14$ at the reference energy $E_0 = 246$ MeV, a curvature parameter around the peak $\beta = 0.19 \pm 0.13$, and a TS = 156. We used a likelihood ratio test to check the PL model (null hypothesis) against the LP model (alternative hypothesis). These values may be compared by defining the curvature test statistic $TS_{curve} = TS_{LP} - TS_{PL} = 1$, meaning that we have no statistical evidence of a curved spectral shape.

In Fig. 2, we show the light curve for the period 2015 December 11–2016 January 9 (MJD 57367–57396), with 1-d (top panel), 12-h (middle panel), and 6-h (bottom panel) time bins. For each time bin, the spectral parameters of PKS 1502+036 and all sources within 10° of it were frozen to the values resulting from the likelihood analysis over the entire period. In the following analysis of the sub-daily light curves, we fixed the flux of the diffuse emission components at the value obtained by fitting the data over the respective daily time bins.

The daily peak of the emission was observed on 2015 December 20 (MJD 57376) with a flux of $(93 \pm 19) \times 10^{-8}$ ph cm^{-2} s^{-1} in the 0.1–300 GeV energy range, 20 times higher than the average flux over the whole period of *Fermi*-LAT observations. The corresponding apparent isotropic γ-ray luminosity peak is $(2.9 \pm 0.6) \times 10^{47}$ erg s^{-1}. Leaving the photon index free to vary the value obtained is $\Gamma = 2.54 \pm 0.04$, indicating that no significant spectral change is detected during the high state on both daily and monthly time-scales. On a 12 and 6-h time-scale, the observed peak flux is $(122 \pm 28) \times 10^{-8}$ and $(172 \pm 40) \times 10^{-8}$ ph cm^{-2} s^{-1}, respectively. The maximum value on a 3-h time-scale (light curve not shown) was observed on December 20 between 1:00 and 4:00 UT with a flux of $(237 \pm 71) \times 10^{-8}$ ph cm^{-2} s^{-1}, corresponding to an apparent isotropic γ-ray luminosity of $(7.3 \pm 2.1) \times 10^{47}$ erg s^{-1}.

After this main flux peak, a secondary peak was observed in the daily light curve on 2015 December 30, with a flux of $(38 \pm 13) \times 10^{-8}$ ph cm^{-2} s^{-1}. By means of the `gtsrcprob` tool, we estimated that the highest energy photon emitted by PKS 1502+036 (with probability > 90 per cent of being associated with the source) was observed on 2009 October 30 at a distance of 0.°05 from PKS 1502+036 with an energy of 21.1 GeV. Analysing the LAT data collected over 2008 August–2016 March in the 10–300 GeV energy range with a PL, the fit yielded a TS = 12, in agreement with the First *Fermi*-LAT catalogue of sources above 10 GeV (1FHL; Ackermann et al. 2013), in which the source is not reported. The 2σ upper limit is 4.4×10^{-11} ph cm^{-2} s^{-1} (assuming a photon index $\Gamma_\gamma = 3$).

3 *Swift* AND *XMM–Newton* OBSERVATIONS

3.1 *Swift* data: analysis and results

The *Swift* satellite (Gehrels et al. 2004) carried out 12 observations of PKS 1502+036 between 2009 July and 2016 January 22. The observations were performed with all three instruments on board: the X-ray Telescope (XRT; Burrows et al. 2005, 0.2–10.0 keV), the Ultraviolet/Optical Telescope (UVOT; Roming et al. 2005, 170–600 nm) and the Burst Alert Telescope (BAT; Barthelmy et al. 2005, 15–150 keV).

The hard X-ray flux of this source turned out to be below the sensitivity of the BAT instrument for such short exposures and therefore the data from this instrument will not be used. Moreover, the source was not present in the *Swift* BAT 70-month hard X-ray catalogue (Baumgartner et al. 2013).

The XRT data were processed with standard procedures (XRTPIPELINE v0.13.2), filtering, and screening criteria by using the HEASOFT package (v6.18). The data were collected in photon counting mode in all the observations. The source count rate was low

Table 1. Log and fitting results of *Swift*–XRT observations of PKS 1502+036 using a PL model with N_H fixed to Galactic absorption.

Date (UT)	MJD	Net exposure time (s)	Photon index (Γ_X)	Flux 0.3–10 keV[a] ($\times 10^{-13}$ erg cm^{-2} s^{-1})
2009-July-25	55037	4662	1.6 ± 0.3	5.1 ± 0.7
2012-April-25	56042	4807	1.7 ± 0.4	4.0 ± 0.7
2012-May-25	56072	4635	1.9 ± 0.4	4.0 ± 0.7
2012-June-25	56103	5142	2.2 ± 0.4	3.8 ± 0.8
2012-August-07/08	56146/7	4925	2.1 ± 0.4	4.7 ± 0.8
2015-December-22	57378	2772	1.5 ± 0.4	6.7 ± 0.7
2015-December-25	57381	2195	1.3 ± 0.5	6.4 ± 0.6
2016-January-01	57388	1768	1.0 ± 0.5	11.6 ± 0.6
2016-January-08	57395	2213	1.8 ± 0.5	6.3 ± 0.7
2016-January-14	57401	2680	1.6 ± 0.5	7.9 ± 0.6

Note. [a]Unabsorbed flux

Table 2. Results of the *Swift*–UVOT data for PKS 1502+036. Upper limits are calculated when the analysis provided a detection significance $< 3\sigma$.

Date (UT)	MJD	v	b	u	$w1$	$m2$	$w2$
2009-July-25	55037	> 18.63	19.16 ± 0.25	18.38 ± 0.18	18.40 ± 0.16	18.22 ± 0.16	18.44 ± 0.12
2012-April-25	56042	18.65 ± 0.37	19.64 ± 0.36	18.87 ± 0.26	18.90 ± 0.22	18.74 ± 0.10	18.54 ± 0.12
2012-May-25	56072	18.68 ± 0.34	19.46 ± 0.28	18.64 ± 0.06	18.29 ± 0.14	18.45 ± 0.16	18.25 ± 0.09
2012-June-25	56103	> 18.57	19.07 ± 0.27	18.72 ± 0.30	18.45 ± 0.08	18.26 ± 0.16	18.54 ± 0.13
2012-August-07	56146	18.33 ± 0.27	>19.65	19.28 ± 0.35	18.51 ± 0.16	18.74 ± 0.19	18.39 ± 0.10
2012-August-08	56147	18.64 ± 0.39	19.22 ± 0.39	18.63 ± 0.30	19.12 ± 0.33	18.48 ± 0.18	18.48 ± 0.12
2015-December-22	57378	18.31 ± 0.24	18.45 ± 0.16	18.09 ± 0.16	17.83 ± 0.10	17.88 ± 0.07	18.14 ± 0.08
2015-December-25	57381	> 18.29	> 19.23	18.55 ± 0.26	18.54 ± 0.19	18.14 ± 0.13	18.91 ± 0.16
2016-January-01	57388	> 17.99	> 19.17	> 20.12	18.38 ± 0.19	18.39 ± 0.17	18.41 ± 0.12
2016-January-08	57395	> 18.47	18.90 ± 0.22	18.70 ± 0.25	18.28 ± 0.15	18.31 ± 0.15	18.29 ± 0.10
2016-January-14	57401	> 18.16	19.10 ± 0.30	18.27 ± 0.21	18.17 ± 0.16	18.35 ± 0.17	18.17 ± 0.08
2016-January-22	57409	> 17.69	> 18.81	18.39 ± 0.32	18.04 ± 0.20	18.00 ± 0.19	18.22 ± 0.16

(< 0.5 counts s^{-1}); thus pile-up correction was not required. The data collected during 2012 August 7 and 8 were summed in order to have enough statistics to obtain a good spectral fit. Source events were extracted from a circular region with a radius of 20 pixels (1 pixel $\sim$ 2.36 arcsec), while background events were extracted from a circular region with radius of 50 pixels far away from the source region. Ancillary response files were generated with XRTMKARF, and account for different extraction regions, vignetting and point spread function corrections. We used the spectral redistribution matrices v014 in the Calibration data base maintained by HEASARC. Considering the low number of photons collected (< 200 counts), the spectra were rebinned with a minimum of 1 count per bin and we used Cash statistics (Cash 1979). We fitted the spectrum with an absorbed PL using the photoelectric absorption model `tbabs` (Wilms, Allen & McCray 2000), with a neutral hydrogen column density fixed to its Galactic value (3.93×10^{20} cm^{-2}; Kalberla et al. 2005). On 2016 January 22, the source was detected at a 2σ level with only five photons, therefore the spectrum is not fitted. The results of the fit are reported in Table 1. The unabsorbed fluxes in the 0.3–10 keV energy range are reported in Figs 4 and 5.

During the *Swift* pointings, the UVOT instrument observed PKS 1502+036 in all its optical (v, b and u) and UV ($w1$, $m2$ and $w2$) photometric bands (Poole et al. 2008; Breeveld et al. 2010). We analysed the data using the `uvotsource` task included in the HEASOFT package (v6.18). Source counts were extracted from a circular region of 5 arcsec radius centred on the source, while background counts were derived from a circular region of 10 arcsec radius in a nearby source-free region. The observed magnitudes are reported in Table 2. Upper limits are calculated when the analysis provided a detection significance $< 3\sigma$. The UVOT flux densities, corrected for extinction using the $E(B-V)$ value of 0.041 from Schlafly & Finkbeiner (2011) and the extinction laws from Cardelli, Clayton & Mathis (1989), are reported in Figs 4 and 5.

3.2 *XMM–Newton* data: analysis and results

XMM–Newton (Jansen et al. 2001) observed PKS 1502+036 on 2012 August 7 for a total duration of 17 ks (observation ID 0690090101, PI: Foschini). The EPIC pn and the EPIC MOS cameras (MOS1 and MOS2) were operated in the full-frame mode. The data were reduced using the *XMM–Newton* Science Analysis System (SAS v15.0.0), applying standard event selection and filtering. Inspection of the background light curves showed that no strong flares were present during the observation, with good exposure times of 13.5, 16.8 and 16.9 ks for the pn, MOS1 and MOS2, respectively. For each of the detectors, the source spectrum was extracted from a circular region of radius 32 arcsec centred on the source, and the background spectrum from a nearby region of radius 32 arcsec on the same chip. All the spectra were binned to contain at least 25 counts per bin to allow for χ^2 spectral fitting.

All spectral fits were performed over the 0.4–10 keV energy range using XSPEC v.12.9.0. The energies of spectral features are quoted in the source rest frame, while plots are in the observer frame. All errors are given at the 90 per cent confidence level. Although we present only the fits to the EPIC-pn, the results were cross-checked for consistency with the EPIC-MOS spectra. Galactic absorption was included in all fits using the `tbabs` model. The results of the fits are presented in Table 3. A simple PL model is sufficient to describe the data, although some residuals are present

Table 3. Fits to the 0.4–10 keV *XMM–Newton* EPIC-pn spectra of PKS 1502+036. Galactic absorption was included in all fits.

Model	Parameter	Value
Power law	Γ	1.9 ± 0.1
	Norm	$5.4 \pm 0.3 \times 10^{-5}$
	χ^2/dof	46/39
Broken power law	Γ_1	2.2 ± 0.3
	$E_{\rm break}$(keV)	$1.6^{+1.1}_{-0.5}$
	Γ_2	$1.5^{+0.2}_{-0.6}$
	Norm	$5.2^{+0.5}_{-0.6} \times 10^{-5}$
	χ^2/dof	31/37

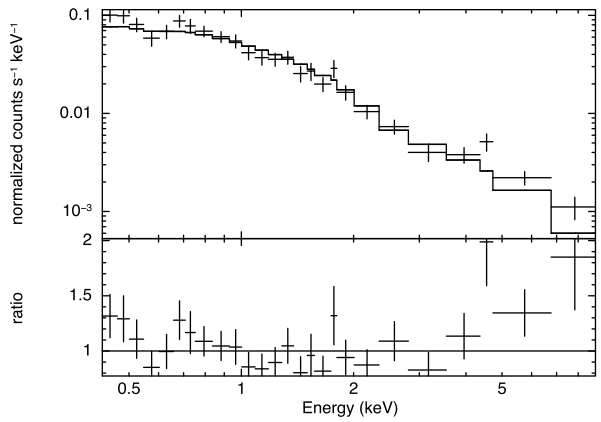

Figure 3. Data and models (upper panel), and data-to-model ratio (lower panel) for the *XMM–Newton* EPIC-pn observation of PKS 1502+036 on 2012 August 7 using a PL model.

at low and high energies (Fig. 3). The EPIC-pn flux estimated in the 0.3–10 keV energy range is $(4.0 \pm 0.4) \times 10^{-13}$ erg cm^{-2} s^{-1}. There is no significant detection of an Fe line in the spectrum, with a 90 per cent upper limit on the equivalent width of 411 eV for a narrow emission line at 6.4 keV.

An improvement of the fit was obtained by using a broken PL. Applying an F-test the probability of obtaining such improvement by chance is 7×10^{-4}. This can be an indication of the presence of both a soft X-ray excess below ∼2 keV and a relativistic jet component at higher energies, as observed in the γ-ray NLSy1 PMN J0948+0022 (D'Ammando et al. 2014). However, the uncertainties on the photon index and flux are quite large (Table 3).

4 OPTICAL AND RADIO OBSERVATIONS

4.1 Optical CRTS data

PKS 1502+036 has been monitored in 2008–2016 by the CRTS[3] (Drake et al. 2009; Djorgovski et al. 2011), using the 0.68 m Schmidt telescope at Catalina Station, AZ, and an unfiltered CCD. The typical cadence is to obtain four exposures separated by 10 min in a given night; this may be repeated up to four times per lunation, over a period of ∼6 to 7 months each year, while the field is observable. Photometry is obtained using the standard Source-Extractor package (Bertin & Arnouts 1996), and transformed from the unfiltered instrumental magnitude[4] to Cousins V by $V = V_{\rm CSS} + 0.31 (B - V)^2 + 0.04$. We averaged the values obtained during the same observing night. During the CRTS monitoring, the source showed a variability amplitude of 0.7 mag, changing between 18.89 and 18.19 mag. The CRTS flux densities, corrected for extinction using the $E(B-V)$ value of 0.041 from Schlafly & Finkbeiner (2011) and the extinction laws from Cardelli et al. (1989), are reported in Figs 4 and 5.

4.2 Radio OVRO data

As part of an ongoing blazar monitoring programme, the OVRO 40 m radio telescope has observed PKS 1502+036 at 15 GHz regularly during 2008–2016 (Richards et al. 2011). This monitoring programme includes over 1900 known and likely γ-ray loud blazars above declination −20°. The sources in this programme are observed in total intensity twice per week with a 4 mJy (minimum) and 3 per cent (typical) uncertainty in their flux densities. Observations are performed with a dual-beam (each 2.5 arcmin FWHM) Dicke-switched system using cold sky in the off-source beam as the reference. Additionally, the source is switched between beams to reduce atmospheric variations. In 2014 May, a new pseudo-correlation receiver was installed on the 40 m telescope and the fast gain variations are corrected using a 180° phase switch instead of a Dicke switch. The performance of the new receiver is very similar to the old one and no discontinuity is seen in the light curves. The absolute flux density scale is calibrated using observations of 3C 286, adopting the flux density (3.44 Jy) from Baars et al. (1977). This results in about a 5 per cent absolute scale uncertainty, which is not reflected in the plotted errors. Flux densities at 15 GHz are reported in Figs 4 and 5. PKS 1502+036 was observed to be variable at 15 GHz during the OVRO monitoring, with a flux density spanning from (282 ± 9) mJy (at MJD 57109) to (749 ± 10) mJy (at MJD 57399).

5 DISCUSSION

5.1 Multifrequency variability

Multiwavelength follow-ups of γ-ray flares are crucial for investigating possible connections between the γ-ray high-activity states and the variability observed in different energy bands. In Fig. 4, we compare the γ-ray light curve obtained by *Fermi*-LAT during 2008 August–2016 March with the X-ray (0.3–10 keV), UV ($w1$, $m2$ and $w2$ filters), optical (u, b and v filters), and radio (15 GHz) light curves obtained by *Swift*, CRTS and OVRO. A zoom of the multifrequency light curve during the high-activity period (i.e. 2015 September 27–2016 March 24, MJD 57292–57471) is shown in Fig. 5.

PKS 1502+036 showed no significant increase in the γ-ray activity during 2008 August–2015 September. The average LAT spectrum accumulated over 2008 August–2016 March is well described by a PL with a photon index of $\Gamma = 2.62 \pm 0.04$. This photon index is similar to the average value observed for Flat Spectrum Radio Quasar (FSRQ) and steep spectrum radio quasars during the first four years of *Fermi*-LAT operation ($\Gamma = 2.44 \pm 0.20$ and 2.42 ± 0.10, respectively; Ackermann et al. 2015) rather than BL Lac objects ($\Gamma = 2.01 \pm 0.25$). The average apparent isotropic γ-ray

[3] http://crts.caltech.edu

[4] http://nesssi.cacr.caltech.edu/DataRelease/FAQ2.html#improve

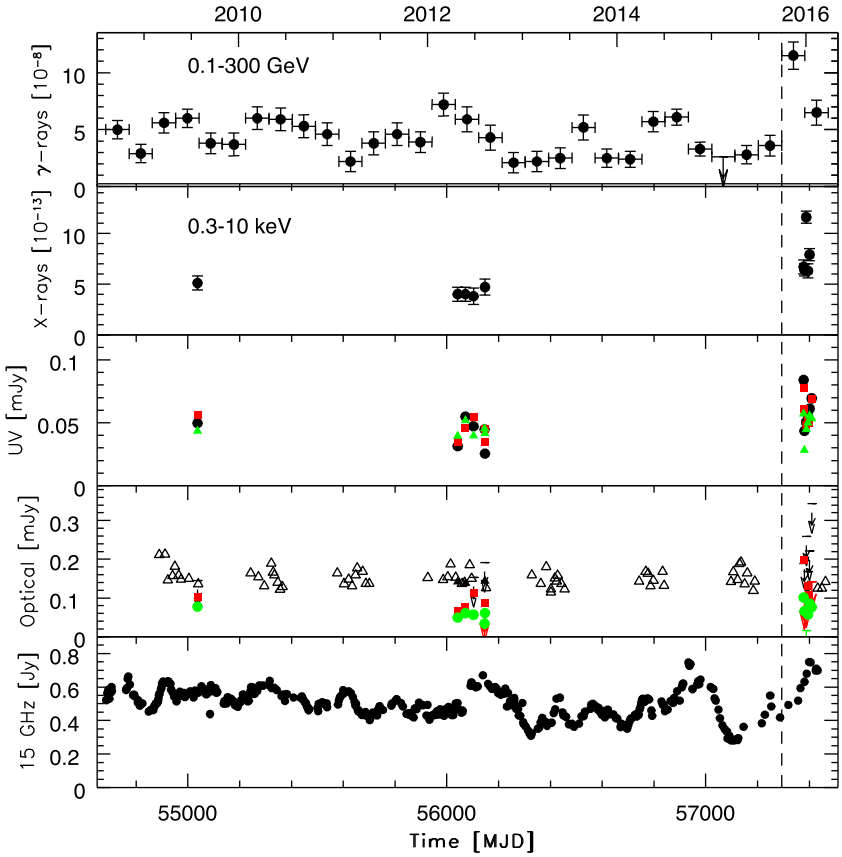

Figure 4. Multifrequency light curve for PKS 1502+036. The period covered is 2008 August–2016 March. The data sets were collected (from top to bottom) by *Fermi*-LAT (γ-rays; in units of 10^{-8} ph cm^{-2} s^{-1}), *Swift*–XRT (0.3–10 keV; in units of 10^{-13} erg cm^{-2} s^{-1}), *Swift*–UVOT (*w*1, *m*2, *w*2 bands, shown as circles, triangles, and squares, respectively; in units of mJy), *Swift*–UVOT (*v*, *b*, *u* bands, shown as filled triangles, circles, and squares, respectively; in units of mJy), CRTS (*V* band, shown as open triangles; in units of mJy), and OVRO (15 GHz, in units of Jy). The vertical dashed line indicates the beginning of the period shown in detail in Fig. 5.

luminosity of PKS 1502+036 is $(1.3 \pm 0.1) \times 10^{46}$ erg s^{-1} in the 0.1–300 GeV range, a typical value for an FSRQ (Ackermann et al. 2015).

An increase in activity was observed in the period 2015 September 29–December 25, with a 90-d averaged flux (0.1–300 GeV) of $(11.5 \pm 1.2) \times 10^{-8}$ ph cm^{-2} s^{-1}. No significant spectral change is detected during this high state, with a photon index of $\Gamma = 2.57 \pm 0.11$. The γ-ray flux increased by a factor of 4 in 5 d after 2015 mid-December (Fig. 5). On a daily time-scale, the peak of activity was detected on 2015 December 20 (MJD 57376), with a flux of $(93 \pm 19) \times 10^{-8}$ ph cm^{-2} s^{-1}, compatible with the daily peak values observed in the other γ-ray-emitting NLSy1 (e.g. SBS 0846+513, PMN J0948+0022, and 1H 0323+342; Carpenter & Ojha 2013; D'Ammando et al. 2013c, 2015a). At the peak of the activity, a maximum value of $(7.3 \pm 2.1) \times 10^{47}$ erg s^{-1} was observed on a 3-h time-scale. Such a high value, together with the radio spectral variability and the one-sided structure observed on parsec scale (D'Ammando et al. 2013b), suggests the presence of a relativistic jet with Doppler factors as large as in FSRQ.

PKS 1502+036 was observed in X-rays by *Swift*/XRT in a bright state during 2015 December–2016 January, with a flux a factor of 1.5–3 higher than in the 2012 observations (Table 1). X-ray spectra of NLSy1 are usually characterized by a soft photon index, i.e. $\Gamma_X > 2$ (e.g. Boller, Brandt & Fink 1996). The photon index during the high-activity period shows a moderate hardening and is always $\Gamma_X < 2$, suggesting the presence of an important contribution from the relativistic jet, as observed for other γ-ray emitting NLSy1 (e.g. D'Ammando et al. 2013c, 2015a). A very hard photon index of $\Gamma_X \sim 1$ was observed on 2016 January 1, but no conclusive evidence can be drawn due to the large uncertainties. The high flux observed during that observation is mainly due to the very hard Γ_X estimated.

The X-ray spectrum of PKS 1502+036 observed by *XMM–Newton* is quite well reproduced by a single PL with photon index $\Gamma_X = 1.9 \pm 0.1$, although some residuals at low and high energies are visible, favouring a broken PL. The residuals at low energies may be the hint of soft X-ray excess, which is a usual feature in the X-ray spectrum of NLSy1 (Grupe et al. 2010) and already detected in the *XMM–Newton* spectrum of the γ-ray NLSy1 PMN J0948+0022 (D'Ammando et al. 2014). In the same way, the residuals observed at high energies may be an indication of the presence of an Fe line in the X-ray spectrum. In this context, the better fit obtained with a broken PL model might indicate that the emission from the jet dominates above ∼2 keV, while a soft X-ray excess is present in the low-energy part of the X-ray spectrum. Unfortunately, during the *XMM–Newton* observation, the flux was too low and the observation time relatively short for detecting both the soft X-ray excess and the Fe line. As for the γ-ray NLSy1 PKS 2004−447 (see Orienti et al. 2015), deeper observations are needed for investigating in detail the presence of these features in the X-ray spectrum of PKS 1502+036.

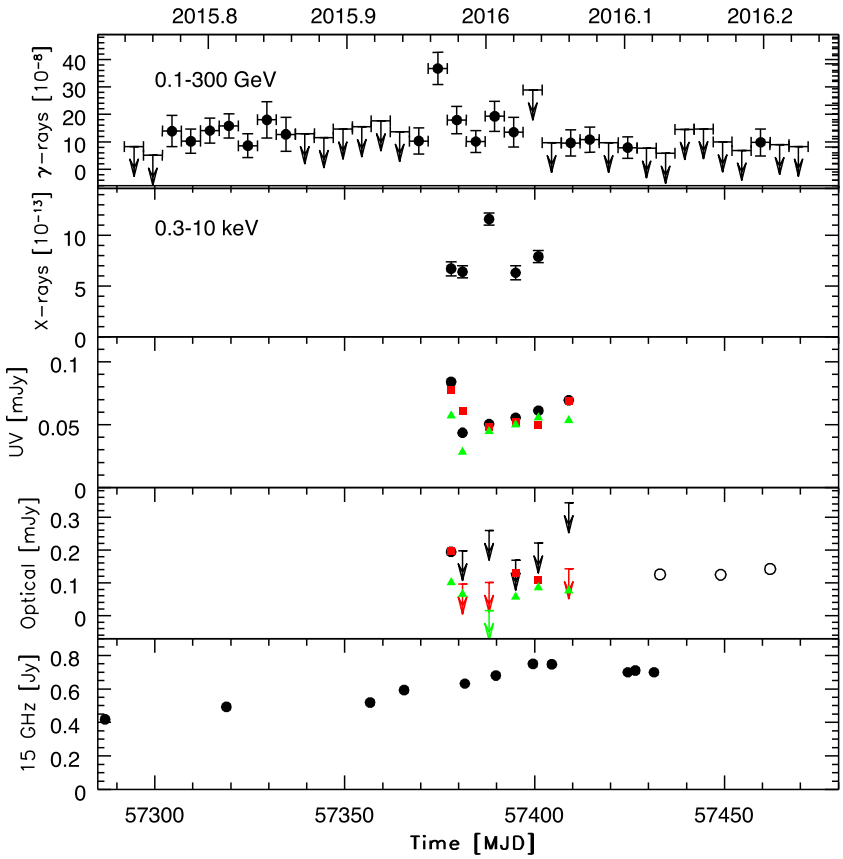

Figure 5. Multifrequency light curve for PKS 1502+036. The period covered is 2015 September 29–2016 March 24. The data sets were collected (from top to bottom) by *Fermi*-LAT (γ-rays, with 5-d time bins; in units of 10^{-8} ph cm^{-2} s^{-1}), *Swift*–XRT (0.3–10 keV; in units of 10^{-13} erg cm^{-2} s^{-1}), *Swift*–UVOT ($w1$, $m2$, $w2$ bands, shown as circles, triangles, and squares, respectively; in units of mJy), *Swift*–UVOT (v, b, u bands, shown as filled circles, triangles, and squares, respectively; in units of mJy), CRTS (v band, shown as open circles; in units of mJy), and OVRO (15 GHz, in units of Jy).

During the *Swift* observation performed in 2015 December 22, the UV and optical emission reached a maximum soon after the γ-ray peak, suggesting a common origin for the multifrequency variability. The variability amplitude (calculated as the ratio between the maximum and minimum flux density) is 1.7, 3.0, 3.1, 3.4, 2.2 and 2.0 in the $v, b, u, w1, m2$ and $w2$ bands, respectively. The decrease of amplitude variability in the $m2$ and $w2$ filters may be due to the presence of an accretion disc that dilutes the jet emission in that part of the spectrum, as already observed for FSRQ (e.g. Raiteri et al. 2012) and the γ-ray NLSy1 PMN J0948+0022 (D'Ammando et al. 2015a).

The analysis of the 15 GHz light curve shows some flux density variability. In particular, during 2008 August–2016 March, PKS 1502+036 showed three outbursts: in 2012 April, 2014 October and 2016 January. The first two radio outbursts seem to be related to an increase of the γ-ray flux by a factor of 2 at the beginning of 2012 and in mid-2014. After the 2014 October outburst, the flux density decreased until April 2015 when it reached the minimum value. Then, it increased again for several months, and peaked on 2016 January 12, about three weeks after the peak of the γ-ray activity. The third outburst showed the largest amplitude variability ($\sim$2.7) in the radio light curve, reaching the highest flux density at 15 GHz for this source so far.

5.2 Radio and γ-ray connection in 2015–2016

Following Valtaoja et al. (1999), we estimate the variability timescale Δt on the basis of the radio data. For Δt, we assume the time interval between the minimum and maximum radio flux density of the outburst $|\Delta S|$. This assumption implies that the minimum flux density corresponds to a stationary underlying component and the variation is due to a transient component. Taking into consideration the time dilation due to the cosmological redshift, we find that the intrinsic time lag is $\Delta\tau = \Delta t/(1+z)$, while the intrinsic flux density variation at the observed frequency is $|\Delta S_i| = |\Delta S| \times (1+z)^{1-s}$ ($S_\nu \propto \nu^{-s}$).

Following D'Ammando et al. (2013b), we derive the rest-frame variability brightness temperature from

$$T'_{\rm B} = \frac{2}{\pi k}\frac{|\Delta S| d_{\rm L}^2}{\Delta t^2 \nu^2 (1+z)^{1+s}}, \quad (1)$$

where k is the Boltzmann constant, ν is the observing frequency, and s is the spectral index. During the outburst, we have $\Delta S = 467$ mJy and $\Delta t = 290$ d. If, in equation (1), we consider these values, and we assume $s = 0.3$, i.e. the average value obtained by fitting the optically thin spectrum (see D'Ammando et al. 2013b), we obtain $T'_{\rm B} \sim 4.6 \times 10^{12}$ K, which exceeds the value derived for the Compton catastrophe. Assuming that such a high value is due to Doppler boosting, we can estimate the variability Doppler factor $\delta_{\rm var}$, by means of

$$\delta_{\rm var} = \left(\frac{T'_{\rm B}}{T_{\rm int}}\right)^{1/(3+s)}, \quad (2)$$

where $T_{\rm int}$ is the intrinsic brightness temperature. Assuming a typical value $T_{\rm int} = 5 \times 10^{10}$ K, as derived by e.g. Readhead (1994) and

Lähteenmäki & Valtaoja (1999), we obtain $\delta_{\rm var} = 3.9$. For the radio outburst which occurred on 2012 July, a $\delta_{\rm var} = 6.6$ was obtained (D'Ammando et al. 2013b). If we consider as the radio outburst the period MJD 57286–57399, we have $\Delta S = 331$ mJy and $\Delta t = 113$ d. In that case, we obtain $T'_{\rm B} \sim 2.1 \times 10^{13}$ K, corresponding to a $\delta_{\rm var} = 6.2$, comparable to the value obtained for the 2012 July outburst. As a comparison, for the γ-ray-emitting NLSy1 SBS 0846+513 and PMN J0948+0022, a variability Doppler factor of 11 and 8.7 was reported in D'Ammando et al. (2013c) and Angelakis et al. (2015), respectively.

We observed a delay of 22 d between the γ-ray and 15 GHz radio peak, which corresponds to 15.6 d in the source's frame. By analysing γ-ray and radio 15 GHz data for a sample of 183 sources, Pushkarev, Kovalev & Lister (2010) found that the γ-ray/radio delay ranges between 1 and 8 months in the observer's frame, with a peak at ∼1.2 months in the source's frame.

Following Pushkarev et al. (2010), we computed the de-projected distance between the γ-ray-emitting region (r_γ) and the radius of the radio core ($r_{\rm c}$) at 15 GHz:

$$\Delta r = r_{\rm c} - r_\gamma = \frac{\beta_{\rm app} c \Delta t^{\rm source}_{{\rm R}-\gamma}}{\sin\theta}, \quad (3)$$

where $\beta_{\rm app}$ is the apparent jet speed, $\Delta t^{\rm source}_{{\rm R}-\gamma}$ is the radio to γ-ray time delay in the source's frame (γ-ray leading) and θ is the viewing angle. In the case of PKS 1502+036, by considering a $\Delta t^{\rm source}_{{\rm R}-\gamma} = 15.6$ d, and $\theta = 3^\circ$, as assumed in Abdo et al. (2009b) and Paliya & Stalin (2016), we obtain $\Delta {\rm r} = 7.6 \times 10^{17} \times \beta_{\rm app}$. Assuming $\beta_{\rm app} = 1.1$, as estimated by Lister et al. (2016), we obtain $\Delta {\rm r} = 8.4 \times 10^{17}$ cm, i.e. 0.27 pc. However, this apparent velocity was derived during a period without significant γ-ray outbursts. If we assume a $\beta_{\rm app} = 10$, similar to the values estimated for the γ-ray NLSy1 SBS 0846+513, 1H 0323+342 and PMN J0948+0022 (D'Ammando et al. 2013c; Lister et al. 2016), we obtain $\Delta {\rm r} = 7.6 \times 10^{18}$ cm, i.e. 2.5 pc.

To evaluate the distance between the γ-ray-emitting region and the jet base, we estimate the radius of the synchrotron self-absorbed radio core at 15 GHz. At any given frequency, the core is the surface where the optical depth τ is close to unity. Therefore, the apparent position of this unit-opacity surface depends on observing frequency (e.g. Königl 1981). In this scenario, we can estimate the size of 15-GHz core, $\theta_{\rm SSA}$ (mas) by

$$\theta_{\rm SSA} \sim f(s)^{5/4} \left(\frac{B}{G}\right)^{1/4} \left(\frac{\nu}{\rm GHz}\right)^{-5/4} \left(\frac{S}{\rm Jy}\right)^{1/2} \left(\frac{1+z}{\delta}\right)^{1/4}, \quad (4)$$

where B is the magnetic field, S is the flux density at the frequency ν, z is the redshift, δ is the Doppler factor and $f(s)$ is a function that depends slightly on s (e.g. Kellermann & Pauliny-Toth 1981).

We assume that the magnetic field is in equipartition:

$$B \sim \left(\frac{c_{12} L}{V}\right)^{2/7}, \quad (5)$$

where L is the radio luminosity, V the volume and $c12$ a constant that is tabulated in Pacholczyk (1970) and depends on the spectral index and the upper and lower cut-off frequencies. By equating 4 and 5 (see Appendix A), we obtain the size that a source with the given flux density and frequency at the synchrotron self-absorption turnover must have to be in equipartition.

For PKS 1502+036, by considering the flux density reached at the peak of the flare (0.749 Jy), and assuming $\delta = 3.9$, as derived by equation (2) and $s = 0.3$, we obtain a projected 15-GHz core radius of ∼0.053 mas, i.e. ∼0.3 pc, which corresponds to a de-projected radius of ∼5.5 pc. Assuming $\delta = 6.2$, we obtain a de-projected radius slightly smaller than the previous one.

It is worth noting that due to the uncertainties affecting the derivation of some parameters, like the magnetic field and the Dopper factor, this value is intended to provide an order of magnitude estimate of the radio core size, rather than an exact measurement. The result implies that the radio core at 15 GHz is located at parsec distance from the jet base, in agreement with other works (e.g. Pushkarev et al. 2012; Fuhrmann et al. 2014; Karamanavis et al. 2016).

By considering the distance between the γ-ray-emitting region and the 15 GHz radio core estimated in equation (3) for $\beta_{\rm app} = 1.1$ and 10, we locate the γ-ray emission region at a distance between 3.0 and 5.2 pc from the central BH. We can infer the broad-line region (BLR) radius using the $R_{\rm BLR}$–L relation from Bentz et al. (2013). By using the luminosity at 5100 Å L(5100) = 2.3×10^{44} erg s^{-1} (Yuan et al. 2008), we obtain $R_{\rm BLR} = 1.4 \times 10^{17}$ cm, i.e. ∼0.05 pc. Assuming that γ-ray and radio flares are related, and therefore separated by ∼3 weeks, this indicates that the γ-ray-emitting region is also located at parsec scale distance from the jet base and beyond the BLR.

5.3 SED modelling

Estimates for the BH mass for PKS 1502+036 span more than one order of magnitude. Yuan et al. (2008) reported $M_{\rm BH} = 4 \times 10^6$ M$_\odot$, based on a virial mass estimate of its optical spectrum. Abdo et al. (2009b), Calderone et al. (2013) and Paliya & Stalin (2016) found $M_{\rm BH} = 2 \times 10^7$, 2×10^8, and 4.5×10^7 M$_\odot$, respectively, all from modelling the optical/UV SED as an accretion disc. Using the optical spectrum from Yuan et al. (2008) and the BH mass scaling relation from Vestergaard & Peterson (2006), we obtain $M_{\rm BH} = 1.4 \times 10^7$ M$_\odot$ for PKS 1502+036, in agreement with the value reported by Abdo et al. (2009b) and Paliya & Stalin (2016). In the same way, Shaw et al. (2012), using the Mg II line from the Sloan Digital Sky Server spectrum, obtained a BH mass of 2.6×10^7 M$_\odot$. It is worth noting that Yuan et al. (2008) used the BLR radius–luminosity relation from Kaspi et al. (2005) to estimate the mass of the source. This is the reason why their estimate is inconsistent with our value. In our modelling here, we use 4.5×10^7 M$_\odot$ following Paliya & Stalin (2016).

Two radio through γ-ray SED are shown in Fig. 6. The two SED represent an average state, and a high-activity state. Aside from the thermal accretion disc emission, we fit the SED with a standard model for an emitting blob in a relativistic jet aligned with our line of sight, producing synchrotron, synchrotron self-Compton (SSC), and external Compton (EC) emission. The synchrotron component considered is self-absorbed below 10^{11} Hz and thus cannot reproduce the radio emission. This emission is likely from the superposition of multiple self-absorbed jet components (Königl 1981). We also included thermal emission by an accretion disc and dust torus. See Finke, Dermer & Böttcher (2008) and Dermer et al. (2009) for details on the model and formulae used. The variability time was chosen to be about 1 d, consistent with the γ-ray light curve (Fig. 2).

We began by fitting the average state, starting with parameters used by Paliya & Stalin (2016). We only needed to modify their parameters slightly to fit this SED; see the resulting model parameters in Table 4. The Doppler factor is similar to the value used in Abdo et al. (2009b) for modelling an average SED of the source. In this model, most of the optical data are explained by synchrotron

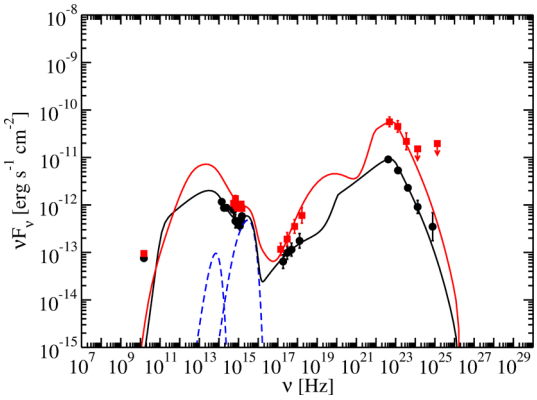

Figure 6. Spectral energy distribution data (squares) and model fit (solid curve) of PKS 1502+036 in flaring activity with the thermal emission components shown as dashed curves. The data points were collected by *Fermi*-LAT (2015 December 18–22), *Swift* (UVOT and XRT, 2015 December 22), and OVRO 40-m (2015 December 25). The SED in the average state reported is shown as circles and includes the *Fermi*-LAT spectrum from the 3FGL catalogue, the *Swift* (UVOT and XRT, 2012 April 25) and OVRO 40-m (2012 April 24) data.

emission; the γ-ray data by EC emission; and the X-ray data by SSC emission. The EC model used is consistent with scattering of dust torus photons constrained by the sublimation radius (Nenkova et al. 2008). We then attempted to fit the high-state SED by varying only the electron distribution parameters from the average state. In this, we were not successful. The γ-ray to optical ratio increases during the flare. By considering that $F_\gamma/F_{\rm optical} \propto (\delta/B)^2$, and assuming the optical emission is from synchrotron and the γ-ray emission is from external Compton, either the Doppler factor or the magnetic field have to change during the flare. This conclusion is fairly robust, since the optical, X-ray and γ-ray data are contemporaneous, and the accretion disc contribution to the optical data is minimal. We chose to slightly modify the magnetic field in order to also fit the high state. Unlike the modelling of Paliya & Stalin (2016), we did not modify both the magnetic field and Doppler factor between the average- and high-state models, choosing instead to modify the minimum number of parameters between states. The optical/UV SED with several model curves for thermal emission from a Shakura–Sunyaev accretion disc is shown in Fig. 7. Within the assumed model, the mass is constrained to be $<10^8$ M$_\odot$.

A Doppler factor $\delta \sim 1$–2, as inferred from the kinematic studies of the MOJAVE images of the source (Lister et al. 2016), would not be able to fit the SED. Such a low value would require a low magnetic field value to fit the γ-ray and optical data. This would make the SSC very large, overproducing the X-ray emission observed, unless the emitting region was made larger, which would conflict with the observed γ-ray variability time-scale. This problem is similar to what is seen for TeV BL Lacs. Bright TeV BL Lac objects have shown jet components with slow apparent speeds (e.g. Piner, Pant & Edwards 2010; Lico et al. 2012), not compatible with Doppler factors inferred from SED modelling (e.g. Abdo et al. 2011). It may be that the SED of PKS 1502+036 could be fit with

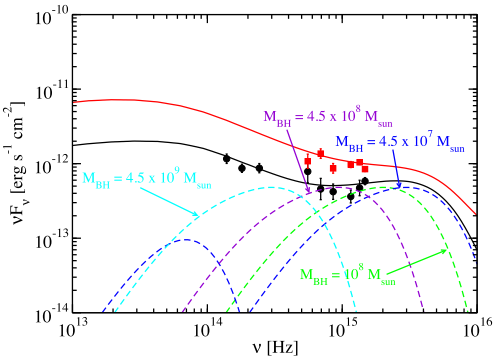

Figure 7. Similar to Fig. 6, but zoomed in on the optical/UV portion of the average spectrum of PKS 1502+036. Model disc emission for different BH masses is shown as the dashed curves. The total (synchrotron + disc) emission is shown as the solid curves. Models with large BH mass do not provide an adequate fit to the UV data of 2012 April 25.

Table 4. Model parameters.

Parameter	Symbol	Average state	High state
Redshift	z	0.409	
Black hole mass (M$_\odot$)	$M_{\rm BH}$	4.5×10^7	
Bulk Lorentz factor	Γ	17	17
Doppler factor	$\delta_{\rm D}$	17	17
Magnetic field (G)	B	0.35	0.27
Variability time-scale (s)	$t_{\rm v}$	7.5×10^4	
Comoving radius of blob (cm)	$R'_{\rm b}$	2.7×10^{16}	2.7×10^{16}
Low-energy electron spectral index	p_1	2.3	2.3
High-energy electron spectral index	p_2	4.5	4.5
Minimum electron Lorentz factor	$\gamma'_{\rm min}$	50	500
Break electron Lorentz factor	$\gamma'_{\rm brk}$	1584	1584
Maximum electron Lorentz factor	$\gamma'_{\rm max}$	1.5×10^5	1.5×10^5
Disc luminosity (erg s^{-1})	$L_{\rm disc}$	6.0×10^{44}	
Inner disc radius (R_g)	$R_{\rm in}$	6.0	
Seed photon source energy density (erg cm^{-3})	$u_{\rm seed}$	7.2×10^{-5}	7.2×10^{-5}
Seed photon source photon energy	$\epsilon_{\rm seed}$	6.0×10^{-7}	6.0×10^{-7}
Dust torus luminosity (erg s^{-1})	$L_{\rm dust}$	7.8×10^{43}	
Dust torus radius (cm)	$R_{\rm dust}$	1.7×10^{18}	
Dust temperature (K)	$T_{\rm dust}$	1200	
Jet power in magnetic field (erg s^{-1})	$P_{\rm j,\,B}$	1.9×10^{44}	1.2×10^{44}
Jet power in electrons (erg s^{-1})	$P_{\rm j,\,e}$	5.1×10^{44}	8.6×10^{44}

a spine-layer model (Ghisellini, Tavecchio & Chiaberge 2005) or a decelerating jet model (Georganopoulos & Kazanas 2003), both of which were proposed to resolve the TeV BL Lac Doppler factor discrepancy. However, we note that the SED of PKS 1502+036 does not resemble a TeV BL Lac, but an FSRQ, where there is no Doppler factor discrepancy. We also note that no MOJAVE observations are collected during the high γ-ray activity period, missing a new superluminal jet component, if ejected.

The γ-ray luminosity and the photon index of PKS 1502+036 and indeed its overall SED are similar to those of FSRQ, or low-synchrotron-peaked BL Lacs. The two SED show a Compton dominance[5] $\sim$10. Note that in modelling the SED of the FSRQ PKS 0537−441, several states could be reproduced by varying only the electron distribution (D'Ammando et al. 2013a). In this way, PKS 1502+036 is similar to the FSRQ PKS 2142−75 (Dutka et al. 2013) and PKS 1424−418 (Buson et al. 2014), and the radio-loud NLSy1 SBS 0846+513 (D'Ammando et al. 2013c) and PMN J0948+0022 (D'Ammando et al. 2015a). However, in PMN J0948+0022 and SBS 0846+513, as well as for PKS 2142−75, the magnetic field increased during the flare with respect to the low or average states. The behaviour of PKS 1502+036 seems to be opposite to the behaviour of these objects. Jet powers for both the average and high states of PKS 1502+036 are near equipartition between the electron and magnetic field energy density, with the electron energy density being slightly higher in both cases.

6 CONCLUSIONS

In this paper, we reported on the observation by the *Fermi*-LAT of flaring γ-ray activity from the NLSy1 PKS 1502+036 in 2015 December. On 2015 December 20, the source reached an apparent isotropic luminosity in the 0.1–300 GeV energy range of $(2.9 \pm 0.6) \times 10^{47}$ erg s^{-1}, which is only a factor of 2 to 3 lower than those reached by the NLSy1 SBS 0846+513 and PMN J0948+0022 during a flare (D'Ammando et al. 2013c, 2015a). On a 3-h time-scale, the source reached a peak flux of $(237 \pm 71) \times 10^{-8}$ ph cm^{-2} s^{-1}, corresponding to an apparent isotropic luminosity of $(7.3 \pm 2.1) \times 10^{47}$ erg s^{-1}.

The average photon index ($\Gamma_\gamma = 2.62 \pm 0.04$) and apparent isotropic luminosity ($L_\gamma = 1.3 \pm 0.1 \times 10^{46}$ erg s^{-1}) estimated over 2008 August 5–2016 March 24 period are similar to the values observed for FSRQ (e.g. Ackermann et al. 2015). No significant change of the γ-ray spectrum was observed during the flare, with a photon index of $\Gamma_\gamma = 2.54 \pm 0.04$.

In addition to the *Fermi*-LAT data, we presented multiwavelength observations of PKS 1502+036 during the period 2008 August–2016 March including *Swift*, *XMM–Newton*, CRTS and OVRO data. An increase of the activity was observed by *Swift* in X-rays, UV and optical on 2015 December 22, just a couple of days after the γ-ray peak, suggesting a common mechanism for the multifrequency variability during the flare.

The source remained in a bright X-ray state during 2015 December–2016 January, with a photon index ranging between 1.0 and 1.8. These values are harder than those observed in 2012, when the source had no significant high-energy outbursts. This suggests a dominant contribution of the jet emission in the X-ray energy range during the high-activity period. The X-ray spectrum collected by *XMM–Newton* in 2012 was quite well fit by a simple PL model, although some residuals are observed at low and high energies. These residuals hint at the presence of a soft X-ray excess and the Fe line, respectively. A better fit was obtained by using a broken PL model, suggesting the presence of two emission components in X-rays, but the uncertainties related to the spectral parameters are quite large. Deeper *XMM–Newton* observations are required for investigating these features in detail.

Flaring activity was also observed in the radio band. At 15 GHz, the peak was detected on 2016 January 12, about three weeks after the γ-ray peak. This radio flare may be the delayed counterpart of the γ-ray one due to opacity effects and the propagation of the shock along the jet. This suggests that the γ-ray-emitting region is placed at $\sim$0.3 pc from the radio 15 GHz radius, and therefore at a distance between 3.0 and 5.2 pc from the central BH, well beyond the BLR.

We compared the broad-band SED of the 2016 flaring activity state with that from an average state of PKS 1502+036 observed in 2012. Both the SED show a Compton dominance $\sim$10. This high value indicates that the EC emission is the main mechanism for producing γ-rays, such as for FSRQ (e.g. Finke 2013), confirming the similarities between γ-ray-emitting NLSy1 and FSRQ. The two SED, with the high-energy bump modelled as an EC component of seed photons from a dust torus, could be modelled by changing both the electron distribution parameters and the magnetic field. An accretion disc is identified in the UV part of the spectrum for the average-activity state, with a luminosity of $L_{\rm disc} = 6 \times 10^{44}$ erg s^{-1}. This value is lower than the luminosity usually observed for FSRQ (e.g. Ghisellini et al. 2014) as well as for the γ-ray NLSy1 PMN J0948+0022 (D'Ammando et al. 2015a). On the other hand, no evidence of thermal emission from the accretion disc has been observed for the γ-ray NLSy1 SBS 0846+513 and PKS 2004−447, with a luminosity of the accretion disc estimated to be very low (10^{42-43} erg s^{-1}; D'Ammando et al. 2013c; Orienti et al. 2015).

No superluminal motion was observed in VLBI images during 2008–2012 (D'Ammando et al. 2013b), with only a sub-luminal component reported in Lister et al. (2016). This is in contrast to the radio spectral variability, the one-sided structure, the observed γ-ray luminosity and the Doppler factor estimated by SED modelling. This result resembles the 'Doppler factor crisis' observed in bright TeV BL Lacs. However, the SED of PKS 1502+036, in particular, the high Compton dominance, does not resemble a TeV BL Lac, but an FSRQ. Future VLBA monitoring of this NLSy1 during flaring activity periods may help to investigate this behaviour.

Assuming a BH mass of 4.5×10^7 M$_\odot$, we obtain a $L_{\rm disc}/L_{\rm Edd} = 0.1$. Within the assumed model, the fit of the disc emission of PKS 1502+036 during the average state constrains the black hole mass to values lower than 10^8 M$_\odot$, and therefore to $L_{\rm disc}/L_{\rm edd} > 4 \times 10^{-2}$, just above the threshold between a radiatively efficient disc, as expected for FSRQ, and an inefficient one, as expected for BL Lacs (Ghisellini et al. 2014). The constraint of 10^8 M$_\odot$ obtained by modelling the optical/UV part of the spectrum of the source confirms that the radio-loud NLSy1, or at least the γ-ray-emitting ones, are blazar-like sources with a BH mass between a few 10^7 M$_\odot$ and a few 10^8 M$_\odot$, therefore at the low end of the blazar distribution. The most powerful jets are found in luminous elliptical galaxies with very massive central BH, where the formation of the relativistic jets is usually triggered by strong merger activity (e.g. Sikora, Stawarz & Lasota 2007; Chiaberge et al. 2015). In this context, it is unlikely that the γ-ray NLSy1 are hosted in disc/spiral

[5] Compton dominance is the ratio of the peak Compton luminosity to peak synchrotron luminosity.

galaxies like the other NLSy1 (e.g. Leon Tavares et al. 2014), but further observations of their host galaxies are needed to unravel the mystery.

ACKNOWLEDGEMENTS

The *Fermi* LAT Collaboration acknowledges generous ongoing support from a number of agencies and institutes that have supported both the development and the operation of the LAT as well as scientific data analysis. These include the National Aeronautics and Space Administration and the Department of Energy in the United States, the Commissariat à l'Energie Atomique and the Centre National de la Recherche Scientifique/Institut National de Physique Nucléaire et de Physique des Particules in France, the Agenzia Spaziale Italiana and the Istituto Nazionale di Fisica Nucleare in Italy, the Ministry of Education, Culture, Sports, Science and Technology (MEXT), High Energy Accelerator Research Organization (KEK) and Japan Aerospace Exploration Agency (JAXA) in Japan, and the K. A. Wallenberg Foundation, the Swedish Research Council and the Swedish National Space Board in Sweden.

Additional support for science analysis during the operations phase is gratefully acknowledged from the Istituto Nazionale di Astrofisica in Italy and the Centre National d'Études Spatiales in France.

We thank the *Swift* team for making these observations possible, the duty scientists, and science planners. The OVRO 40 m monitoring programme is supported in part by NASA grants NNX08AW31G and NNX11A043G, and NSF grants AST-0808050 and AST-1109911. The CSS survey is funded by the National Aeronautics and Space Administration under Grant No. NNG05GF22G issued through the Science Mission Directorate Near-Earth Objects Observations Programme. The CRTS survey is supported by the US National Science Foundation under grants AST-0909182. Based on observations obtained with *XMM–Newton*, an ESA science mission with instruments and contributions directly funded by ESA Member States and NASA. Part of this work was done with the contribution of the Italian Ministry of Foreign Affairs and Research for the collaboration project between Italy and Japan. We thank S. Ciprini, J. Perkins, and the anonymous referee for useful comments and suggestions.

REFERENCES

Abdo A. A. et al., 2009a, ApJ, 699, 976
Abdo A. A. et al., 2009b, ApJ, 707, L142
Abdo A. A. et al., 2010, ApJS, 188, 405
Abdo A. A. et al., 2011, ApJ, 736, 131
Acero F. et al., 2015, ApJS, 218, 23
Acero F. et al., 2016, ApJS, 223, 2
Ackermann M. et al., 2012, ApJS, 203, 4
Ackermann M. et al., 2013, ApJS, 209, 34
Ackermann M. et al., 2015, ApJ, 810, 14
Angelakis M. et al., 2015, A&A, 575A, 55
Atwood W. B. et al., 2009, ApJ, 697, 1071
Atwood W. B. et al., 2013, preprint (arXiv:1303.3514)
Baars W. M., Genzel R., Pauliny-Toth I. I. K., Witzel A., 1977, A&A, 61, 99
Baldi R., Capetti A., Robinson A., Laor A., Behar E., 2016, MNRAS, 458, L69
Barthelmy S. D. et al., 2005, Space Sci. Rev., 120, 143
Baumgartner W. H., Tueller J., Markwardt C. B., Skinner G. K., Barthelmy S., Mushotzky R. F., Evans P., Gehrels N., 2013, ApJS, 207, 19
Bentz M. C. et al., 2016, ApJ, 767, 149
Bertin E., Arnouts S., 1996, A&AS, 117, 393
Blandford R. D., Rees M. J., 1978, in Wolfe A. M., ed., Pittsburgh Conference on BL Lac Objects. Univ. Pittsburgh Press, p. 328
Boller T., Brandt W. N., Fink H., 1996 A&A, 305, 53
Böttcher M., Dermer C. D., 2002, ApJ, 564, 86
Breeveld A. A. et al., 2010, MNRAS, 406, 1687
Burrows D. N. et al., 2005, Space Sci. Rev., 120, 165
Buson S. et al., 2014, A&A, 569, A40
Calderone G., Ghisellini G., Colpi M., Dotti M., 2013, MNRAS, 431, 210
Cardelli J. A., Clayton G. C., Mathis J. S., 1989, ApJ, 345, 245
Carpenter B., Ojha R., 2013, Astronomer's Telegram, 5344
Cash W., 1979, ApJ, 228, 939
Chiaberge M., Gilli R., Lotz J. M., Norman C., 2015, ApJ, 806, 147
D'Ammando F., 2015, Astronomer's Telegram, 8450, 1
D'Ammando F., Ciprini S., 2015, Astronomer's Telegram, 8447, 1
D'Ammando F. et al., 2012, MNRAS, 426, 317
D'Ammando F. et al., 2013a, MNRAS, 431, 2481
D'Ammando F. et al., 2013b, MNRAS, 433, 952
D'Ammando F. et al., 2013c, MNRAS, 436, 191
D'Ammando F. et al., 2014, MNRAS, 438, 3521
D'Ammando F. et al., 2015a, MNRAS, 446, 2456
D'Ammando F., Orienti M., Larsson J., Giroletti M., 2015b, MNRAS, 452, 520
Deo R. P., Crenshow D. M., Kraemer S. B., 2006, AJ, 132, 321
Dermer C. D., Finke J. D., Krug H., Böttcher M., 2009, ApJ, 692, 32
Djorgovski S. G. et al., 2011, preprint (arXiv:1102.5004)
Drake A. J. et al., 2009, ApJ, 696, 870
Dutka M. S. et al., 2013, ApJ, 779, 174
Finke J. D., 2013, ApJ, 763, 134
Finke J. D., Dermer C. D., Böttcher M., 2008, ApJ, 686, 181
Fuhrmann L. et al., 2014, MNRAS, 441, 1899
Gehrels N. et al., 2004, ApJ, 611, 1005
Georganopoulos M., Kazanas D., 2003, ApJ, 594, L27
Ghisellini G., Tavecchio F., Chiaberge M., 2005, A&A, 432, 401
Ghisellini G., Tavecchio F., Maraschi L., Celotti A., Sbarrato T., 2014, Nature, 515, 376
Grupe D., Komossa S. Leighly K. M., Page K. L., 2010, ApJS, 187, 64
Hartman R. C. et al., 1999, ApJS 123, 79
Jansen F. et al., 2001, A&A, 365, L1
Jiang N. et al., 2012, ApJ, 759, L31
Kalberla P. M. W., Burton W. B., Hartmann D., Arnal E. M., Bajaja E., Morras R., Pöppel W. G. L., 2005, A&A, 440, 775
Karamanavis V. et al., 2016, A&A, 590A, 48
Kaspi S., Maoz D., Netzer H., Peterson B. M., Vestergaard M., Jannuzi B. T., 2005, ApJ, 629, 61
Kellermann K. I., Pauliny-Toth I. I. K., 1981, ARA&A, 19, 373
Komatsu E. et al., 2011, ApJS, 192, 18
Konigl A., 1981, ApJ, 243, 700
Lähteenmäki A., Valtaoja E., 1999, ApJ, 521, 493
Leon Tavares J. et al., 2014, ApJ, 795, 58
Lico R. et al., 2012, A&A, 545, 117
Lister M. L. et al., 2016, AJ, 152, 12
Marconi A., Axon D. J., Maiolino R., Nagao T., Pastorini G., Pietrini P., Robinson A., Torricelli G., 2008, ApJ, 678, 693
Marscher A. P., 2010, in Belloni T., ed., Lecture Notes in Physics, Vol. 794. The Jet Paradigm. Springer-Verlag, Berlin, p. 173
Mattox J. R. et al., 1996, ApJ, 461, 396
Nenkova M., Sirocky M. M., Nikutta R., Ivezić Ž., Elitzur M., 2008, ApJ, 685, 160
Nolan P. et al., 2012, ApJS, 199, 31
Orienti M., D'Ammando F., Giroletti M., 2012, preprint (arXiv:1205.0402)
Orienti M., D'Ammando F., Larsson J., Finke J., Giroletti M., Dallacasa D., Isacsson T., Stoby Hoglund J., 2015, MNRAS, 453, 4037
Pacholczyk A. G., 1970, Radio astrophysics. Nonthermal Processes in Galactic and Extragalactic Sources. W. H. Freeman & Co Ltd, San Francisco
Paliya V. S., Stalin C. S., 2016, ApJ, 820, 52

Paliya V. S., Stalin C. S., Kumar B., Kumar B., Bhatt V. K., Pandey S. B., Yadav R. K. S., 2013, MNRAS, 428, 2450
Piner B. G., Pant N., Edwards P. G., 2010, ApJ, 723, 1150
Poole T. S. et al., 2008, MNRAS, 383, 627
Pushkarev A. B., Kovalev Y. Y., Lister M. L., 2010, ApJ, 722, L7
Pushkarev A. B., Hovatta T., Kovalev Y. Y., Lister M. L., Lobanov A. P., Savolainen T., Zensus J. A., A&A, 545, 113
Raiteri C. M. et al., 2012, A&A, 545, A48
Readhead A. C. S., 1994, ApJ, 426, 51
Richards J. L. et al., 2011, ApJS, 194, 29
Roming P. W. A. et al., 2005, Space Sci. Rev., 120, 95
Schlafly E. F., Finkbeiner D. P., 2011, ApJ, 737, 103
Schneider D. P. et al., 2010, AJ, 139, 2360
Shaw M. et al., 2012, ApJ, 748, 49
Sikora M., Stawarz L., Lasota J.-P., 2007, ApJ, 658, 815
Valtaoja E., Lähteenmäki A., Teräsranta H., Lainela M., 1999, ApJS, 120, 95
Vestergaard M., Peterson B. M., 2006, ApJ, 641, 689
Wilms J., Allen A., McCray R., 2000, ApJ, 542, 914
Yuan W., Zhou H. Y., Komossa S., Dong X. B., Wang T. G., Lu H. L., Bai J. M., 2008, ApJ, 685, 801

APPENDIX A: THE SSA RADIO CORE

In Section 5.1, we derived the size which a source with the given flux density and frequency at the synchrotron self-absorption turnover must have to be in equipartition. To do so, we equate the magnetic field strength, $H_{\rm SSA}$, as derived from the self-absorption expression with the equipartition magnetic field. The former is computed by

$$H_{\rm SSA} \sim f(s)^{-5} \left(\frac{\theta_{\rm SSA}}{\rm mas}\right)^{4} \left(\frac{\nu}{\rm GHz}\right)^{5} \left(\frac{S}{\rm Jy}\right)^{-2} \frac{\delta}{(1+z)}\ {\rm G}, \quad \text{(A1)}$$

where $f(s)$ is a function that depends slightly on s (e.g. Kellermann & Pauliny-Toth 1981). The equipartition magnetic field, $H_{\rm eq}$, is obtained by

$$H_{\rm eq} \sim \left(c_{12}\frac{L}{V}\right)^{2/7}, \quad \text{(A2)}$$

where L is the radio luminosity, V the volume, and c_{12} a value tabulated in Pacholcyzk (1970). The radio luminosity is obtained by

$$L = \frac{4\pi D_{\rm L}^2}{(1+z)1-s} \int_{\nu_1}^{\nu_2} S(\nu){\rm d}\nu. \quad \text{(A3)}$$

We approximate the volume of the source component to a sphere which is homogeneously filled by the relativistic plasma:

$$V = \frac{4\pi}{3}\left(\frac{D_{\rm L}}{(1+z)^2}\right)^3 \theta_{\rm eq}^3. \quad \text{(A4)}$$

If in equation (A2) we consider equations (A3) and (A4), we obtain

$$H_{\rm eq} \sim 9\times10^{-7} c_{12}^{2/7} S_0^{2/7} \nu_0^{2s/7} \delta^{\frac{-6-2s}{7}} (1+z)^{\frac{10+2s}{7}} \times D_{\rm L}^{-2/7} \theta_{\rm eq}^{-6/7} c_\nu^{2/7}, \quad \text{(A5)}$$

where S_0 is the flux density in Jy at the frequency ν_0 in Hz, $D_{\rm L}$ is the luminosity distance in Mpc, $\theta_{\rm eq}$ is the radius in mas, $H_{\rm eq}$ is the equipartition magnetic field in G, and c_ν is the result of $\int_{\nu_1}^{\nu_2} \nu^{-s}{\rm d}\nu$.

If we equate equations (A5) and (A1), and considering that $\theta_{\rm SSA} = 2\times\theta_{\rm eq}$, we have

$$\theta_{\rm eq} \sim 5\times10^{8} c_{12}^{1/17} c_\nu^{1/17} S_0^{8/17} \nu_0^{\frac{2s-35}{34}} \delta^{\frac{-13-2s}{34}} \times (1+z)^{\frac{17+2s}{34}} D_{\rm L}^{1/17}. \quad \text{(A6)}$$

This paper has been typeset from a TEX/LATEX file prepared by the author.